Time Accurate Euler Calculations of Vortical Flow over a Delta Wing in Rolling Motion

W. Fritz
EADS Deutschland GmbH, Military Aircraft, Dept. MT632/Build. 70 N
D-81663 München, Germany

M.T. Arthur
DERA, Aerodynamics Department, Küchemann Building, DERA, Ively Road
Farnborough, Hampshire, GU14 0LX, U.K.

F.J. Brandsma
NLR, Theoretical Aerodynamics Dept., P. O. Box 90502
NL-1006 BM-Amsterdam, The Netherlands

K.-A. Bütefisch
DLR AS-GÖ, Bunsenstraße 10
D-37073 Göttingen, Germany

N. Ceresola
Alenia Aeronautica, Gruppo Nuovi Prodotti e Technologi, Corso Marche 41
I-19146 Torino, Italy

Abstract

This paper presents the results of the research work conducted by the participants Alenia (Italy), Dasa (Germany), DERA (United Kingdom), NLR (The Netherlands) and DLR (Göttingen, Germany) in the former European programme WEAG-TA15 within Common Exercise V [1]. The objective of this common exercise was the numerical and experimental investigation of vortex dominated flow about a rolling delta wing and also to provide a data base for further code validation. Numerical calculations with different unsteady Euler methods (central schemes with dissipation, upwind schemes) using a common grid have been performed at a constant rolling rate of ω_r=0.0762 for different angles of incidence: α_0=0°, α_0=10° and α_0=17°. From the numerical results it turns out that the different spatial discretisations lead to characteristic differences mainly in the magnitudes of the vortex induced suction peaks in the unsteady pressure distributions and in the prediction of vortex breakdown.

Introduction

The Western European Armaments Group (WEAG) TA15 programme was a European collaborative programme concerned with the investigation of steady and unsteady vortical flows over military aircraft configurations. A very important component of the WEAG TA15 programme was the "Common Exercises" (CE), which promoted the exchange of knowledge between the participating nations and also aided the development of computational methods through an assessment of their capability in the prediction of vortical flows. Earlier common exercises had concentrated on steady state vortical flow and on the improvement of the capturing of vortical structures in steady flow using solution adaptive methods [2]. Within the last 5 years, the work within WEAG concentrated more and more on the experimental and numerical investigation of unsteady vortical flow. A common exercise dealing with inviscid unsteady flow about a delta wing oscillating in pitch [3] as well as detailed numerical studies [4], [5] have demonstrated the usefulness (and limitations) of unsteady Euler calculations for vortical flow fields. Comparisons of unsteady Euler and unsteady Navier-Stokes results [5], [7] have also shown that the basic unsteady effects in the flow field (variation of the primary vortex including vortex breakdown, phase lag of the flow field) can be predicted by Euler methods.

As the analysis of flow fields about rolling delta wings is of high general interest (the rolling motion produces asymmetric leading-edge vortices which can lead to roll instabilities as has been observed in high performance military aircraft and in ref. [11] for a rolling delta wing at high incidence), the last

Paper presented at the RTO AVT Symposium on "Advanced Flow Management: Part A – Vortex Flows and High Angle of Attack for Military Vehicles", held in Loen, Norway, 7-11 May 2001, and published in RTO-MP-069(I).

Report Documentation Page

Form Approved
OMB No. 0704-0188

1. REPORT DATE	2. REPORT TYPE	3. DATES COVERED
00 MAR 2003	**N/A**	**-**

4. TITLE AND SUBTITLE	5a. CONTRACT NUMBER
Time Accurate Euler Calculations of Vortical Flow Over a Delta Wing in Rolling Motion	5b. GRANT NUMBER
	5c. PROGRAM ELEMENT NUMBER
6. AUTHOR(S)	5d. PROJECT NUMBER
	5e. TASK NUMBER
	5f. WORK UNIT NUMBER
7. PERFORMING ORGANIZATION NAME(S) AND ADDRESS(ES) **NATO Research and Technology OrganisationBP 25, 7 Rue Ancelle, F-92201 Neuilly-Sue-Seine Cedex, France**	8. PERFORMING ORGANIZATION REPORT NUMBER
9. SPONSORING/MONITORING AGENCY NAME(S) AND ADDRESS(ES)	10. SPONSOR/MONITOR'S ACRONYM(S)
	11. SPONSOR/MONITOR'S REPORT NUMBER(S)

12. DISTRIBUTION/AVAILABILITY STATEMENT
Approved for public release, distribution unlimited

13. SUPPLEMENTARY NOTES
Also see: ADM001490, Presented at RTO Applied Vehicle Technology Panel (AVT) Symposium held inLeon, Norway on 7-11 May 2001, The original document contains color images.

14. ABSTRACT

15. SUBJECT TERMS

16. SECURITY CLASSIFICATION OF:			17. LIMITATION OF ABSTRACT	18. NUMBER OF PAGES	19a. NAME OF RESPONSIBLE PERSON
a. REPORT	b. ABSTRACT	c. THIS PAGE			
unclassified	**unclassified**	**unclassified**	**UU**	**14**	

Standard Form 298 (Rev. 8-98)
Prescribed by ANSI Std Z39-18

"Common Exercise" (CE V) of this group has concentrated on the numerical and experimental investigation of the unsteady flow over a 65º swept delta wing in rolling motion at transonic speed. Guided by the experiences of former work on unsteady motions, the numerical investigation was again restricted to unsteady Euler methods. The CE V had to be completed within a strict time frame. Thus each participant for the numerical calculations (Alenia, Dasa, DERA, NLR) was asked to perform unsteady Euler calculations for given test cases using a mandatory grid and a given number of physical time steps per period.

Besides the numerical calculations, DLR-Göttingen has prepared and performed experimental investigations using the new Pressure Sensitive Paint (PSP) technique, which was applied within CE V for the first time to unsteady flow. Both numerical and experimental results should finally give a data base for further code validation, but during the experimental investigations it turned out that there are still some problems with the PSP technique in unsteady flow. Therefore only preliminary experimental results were available at the end of CE V. Details of the experimental investigations are given in [8].

Geometry and Test Conditions

The CE V geometry is the 65° swept model of the TA15 delta wing with sharp leading edge, combined with a symmetric body. It has been designed at DLR for experimental studies of rolling motions. Figure 1 shows this model as it was still under construction. The fuselage starts with a circular cross section at the apex and develops to a constant cross section after some distance from the apex. In order to avoid unwanted additional vortices generated at sharp corners, the fuselage is smoothly faired to the wing geometry. The basic wing geometry is the same geometry which is known as WB1-SLE (aspect ratio A=1.38, symmetric airfoil). The wing root chord of the wind tunnel model is 420 mm.

Figure 2 gives an impression of the computational grid, which was generated at NLR. The grid is of C-O-Type, giving a singular line running from the apex to the upstream boundary and an O-type singularity at the edges of the wake-cut downstream of the trailing edge towards the downstream far-field boundary. The sting is extended to the down stream far-field boundary. The total number of grid points is 72·192·28 = 387022 grid cells. More details about the grid generation can be found in [9].

The test cases for CE V were rolling with constant rolling rate about the body axis at maximum instantaneous angles of attack α_0=0°, α_0=10° and α_0=17°. (The latter two cases have also been investigated in the wind tunnel by the PSP technique). The constant reduced rolling rate, which was restricted by the experimental equipment, was $\omega_r = 2\pi n_0 b/U_\infty = 0.0762$, with U_∞ the free stream velocity, n_0 the physical roll rate (Rps) and b (0.333m) the span of the delta wing. This value of the reduced roll rate corresponds to the physical roll rate of 10 Rps (3600°/s) at the Mach number M_∞=0.8. The above three test cases have been calculated by the participants with a resolution in time of 72 time steps per period in a mandatory grid and starting from a steady solution. All participants used a dual time stepping scheme for time accuracy but used different spatial discretisations (central or upwind).

Numerical Algorithms

At Alenia, the solution algorithm (UNS3D) is based on a finite volume, node centred approach operating on an unstructured grid, using the dual cell approach. The artificial dissipation model is derived from the non-linear dissipation scheme of Jameson, where the dissipation terms in each direction are related to the spectral radii of the inviscid operator. No eigenvalue blending is applied. For the integration in time, the dual time stepping scheme with a five stage Runge Kutta scheme in the inner loop and a second-order backward differencing in time is employed. No multigrid acceleration is used. More details are given in [6].

At Dasa, a Jameson-type in-house developed 3-D single-block structured unsteady Euler code for wing and wing-body combinations was used for the CE V calculations. The dissipation model is the non-isotropic dissipation model of Jameson, but with eigenvalue blending. A modified formulation of the dual time stepping scheme (special treatment of the implicit source term) is used for the time integration and the time derivative is approximated by a second order backward difference. Local time stepping, implicit residual averaging and the multi-grid strategy are used to reduce the residual within each time step. Some test-cases have also been recomputed by the use of the DLR code FLOWer 115 [14], using also the Jameson-type scheme settings.

The computations provided by DERA were performed at the University of Glasgow using the code PMB3D, in which the unsteady Navier-Stokes equations are discretised on a curvilinear multiblock

body-conforming mesh using a fully implicit cell-centred finite volume method. The convective terms are discretised using Osher's upwind scheme. MUSCL variable extrapolation is used to provide second-order accuracy in space with the Van Albada limiter to prevent spurious oscillations around shocks. The linear system of equations formed by the fully implicit method is solved using a Krylov subspace method. Time accuracy is achieved by Jameson's dual time stepping technique. The time derivative is approximated by a second order backward difference.

The NLR CFD simulation model is based on a Discontinuous Galerkin (DG) finite element discretisation of the unsteady Euler equations, which is a mixture of a finite element and an upwind finite volume method. The most relevant feature of the DG finite element method is that equations are solved not only for the mean flow field, but also for the flow field gradients. This results in a very local scheme, because it is not necessary to reconstruct a flow field gradient to achieve second order accuracy, using data in neighbouring elements. The dynamic motion is simulated using a translating-rotating reference frame connected to the configuration and using an Arbitrary Lagrangian Eulerian (ALE) formulation for the additional fluxes due to the moving grid. The discretisation in time is based on a three-point backward implicit time integration method. The non-linear equations of the implicit time integration method are solved with a dual time stepping procedure. Within each implicit time step convergence to steady state is accelerated using a FAS multigrid method and local time stepping in pseudo-time. A more detailed description of the method is given in [4].

All participants have treated the rolling motion as a so-called rigid body motion, which means the use of a rotating grid.

Steady State Results

All the typical characteristics of the different schemes can be seen in the steady solutions, which have been used as initial solution for the unsteady calculations. In the surface pressure contours (Figure 3), the overall agreement between the different solutions is good, except for α=17°, where the NLR solution shows vortex breakdown and the other solutions do not. All solutions show the well known Euler result, that is, the separation along the sharp leading edge is captured by methods based on the Euler equations and the resulting sheet (theoretically a contact discontinuity) rolls up to form a primary vortex rather close to the sharp leading edge. Depending on the numerical scheme this vortex can be very compact (Upwind schemes of the University of Glasgow and NLR) or less compact (central scheme with dissipation of Dasa), which can be seen very clearly in the comparison of the surface pressure distributions in Figure 4. (The experimental data were obtained by DLR applying the PSP technique; more details are given in [8]). In the computed surface pressure distributions, the leeward suction peak is over-predicted and its position is more outboard, which is an effect of the missing secondary vortex. In the experiment, the suction peak seems to be more compact but this is surely an effect of the grid resolution in the Euler calculations, combined with the effect of a missing secondary separation compared to the experiment.

Unsteady results at angle of incidence α=0°

Figure 5 shows the spanwise pressure distributions of the Dasa, NLR and DERA solutions at the cross sections x/c=0.6 and x/c=0.8. All surface pressure distributions are exactly antisymmetric with respect to η=0, resulting in zero lift and in a non zero rolling moment as should be expected for this test case. (It should be noticed that the c_p curves from a given solution cross at η=0.) At the cross section x/c=0.6, there is still no vortex present, whereas at x/c=0.8 a very weak vortex can be recognised in all three solutions. The pressure distributions of the Dasa and NLR solutions are identical. Obviously the numerical dissipation of the Dasa scheme is of no importance in this test case (there is no discontinuity which can be smeared out). The DERA solution shows in both cross sections a lower level of the suction peaks. This is surprising since, in the steady solutions, the Osher upwind scheme has shown higher levels of the suction peaks than any of the other schemes.

Unsteady results at angle of incidence α=10°

For convention, a positive roll velocity means that the right hand side of the wing when looking in the upstream direction is moving upward. Therefore in all the representations of the surface pressure contours, the turning direction is counter clockwise about the body. The section surface pressure distributions are front views so that here the turning direction is clockwise. The rolling moment coefficient is positive when damping a rolling motion with positive roll velocity. (This is not the

common convention but an effect of stand alone flow solvers which associate a positive lift at the positive half of the wing with a positive rolling moment.)

Figure 6 shows the surface pressure contours of the leeward wing side in the horizontal and in the vertical position for the reduced rolling rate ω_r=0.0762 during the third cycle of the simulated roll motion. In the horizontal position, the local angle of attack has its maximum, resulting in well developed leading edge vortices, while at the vertical position the local angle of attack is zero, resulting in a complete vanishing of the leading edge vortices. At all other positions during the motion, there is a continuous variation between these types of the flow field. Figure 6 also shows that there are only very small dynamic effects (very small differences between left and right part of the wing in the horizontal position).The normal force coefficient shows no time lag effect (Figure 7). The extreme values of the pitching moment are predicted by the Dasa and NLR solutions between the vertical and the horizontal position of the wing. This is mainly an effect of the antisymmetric flow field rather than a dynamic effect. Only the rolling moment (Figure 7) shows a considerable rate-induced time history lag: the minimum value is reached with a phase shift of 45° compared to the static case (in the static case the rolling moment passes zero at the horizontal and vertical positions). At a phase angle of about 150° the rolling moment becomes negative, denoting that the vortex at the upward moving leading edge is stronger than the vortex at the downward moving leading edge. Figure 8 shows the unsteady pressure distributions in terms of magnitudes and phase angles of the first three harmonics, based on a cosine-type harmonic analysis. Compared with harmonic pitch oscillations [3], the magnitudes of the higher harmonics are here much larger, though nearly in phase. Besides the natural phase shift of 180° between upper and lower side, the first harmonic shows a negligible phase shift. The second harmonic shows large variations, but in the region of the primary vortices (where the magnitude has a considerable value), the phase angle has values between 10° and 50°. In the regions with large phase angles, the magnitudes of the second harmonic are very small. The phase angle of the third harmonic is hard to analyse, but if the modulo 180° jumps are repaired, it looks similar to the phase angle of the first harmonic: a curve very close to the zero axis for the upper side and a natural shift of 180° between upper and lower sides. In the prediction of the magnitudes, the different schemes show the same characteristics as was discussed for the steady solutions: higher suction peaks from the upwind schemes, somewhat lower suction peaks from the central schemes with dissipation. In the prediction of the phase angle, no characteristic differences between the different schemes can be observed. In the phase shift of the first harmonic, the results of all schemes are identical and also, for the higher harmonics, the results of Dasa, DERA and NLR are very similar over a wide range.

As there is no vortex breakdown present at the conditions of this test case, the dominating effect here is the variation of the local angles of incidence and yaw, and this variation is nearly in phase with the motion. This results in very small phase shifts in the loads, only the rolling moment showing a significant, rate-induced time-history lag. The same effect was also observed in [11] and in [13] for roll oscillations.

Unsteady results at angle of incidence α=17°

The instantaneous surface pressure contours during the third cycle of the motion are shown in Figs. 9 and 11 respectively. At the beginning of the downstroke motion (the wing turns from the horizontal to the vertical position), the solutions of Alenia and Dasa continue to show a burst vortex at the upward turning half of the wing (figure 9). Over this part of the wing, the onset of vortex breakdown occurs during the upstroke motion and is still present in these two solutions. At 60º roll angle, the NLR solution shows very clearly vortex breakdown over the downward moving half of the wing. In the Dasa solution, there is a considerable increase in the pressure ahead of the trailing edge, but the vortex is not yet burst. The vortex breakdown or tendency to breakdown during this part of the motion is due to the increase of slip angle leading to a strengthening of the vortex at the windward side. During the upstroke motion (the wing turns from the vertical to the inverted horizontal position), all solutions show clearly vortex breakdown over the upward turning half of the wing and this vortex breakdown is still present at the horizontal position (Figure 11). During this part of the motion it is the effect of that the vortex is forced to get closer to the surface that induces the breakdown. It is therefore clear that there are large time lags in the vortex breakdown motion relative to the forced rolling motion as was also observed in ref. [12]. In the solutions obtained using the upwind schemes of the University of Glasgow and NLR, the vortex at the horizontal position is still burst, but it has already started to regenerate. In the Alenia and Dasa solutions (central schemes with dissipation), the vortex is still retracting towards the wing apex at the horizontal position, which explains its presence during the downstroke motion.

Figure 10 shows a comparison of instantaneous surface pressure distributions with the preliminary experimental values, which were obtained at DLR using the PSP technique [8]. In the numerical solutions, the upwind schemes show a higher level of the suction peak and also a more compact region of this suction peak than the central scheme of Dasa. As long as no vortex breakdown is present, there are extreme differences between the numerical and the experimental suction peak levels and there are also considerable differences in the midsection of the wing, where in the steady case the agreement between numerical and experimental results was very good (Figure 4). Compared with the steady results (Figs. 4 and 10), the numerical results appear to be consistent, whereas in the experiment there are extreme differences between static and dynamic results which cannot be explained by the rolling motion at such a low rate.

Figure 12 shows the variation of normal force, pitching moment and rolling moment coefficient. The normal force coefficient shows again nearly no phase lag. Although the solutions of Alenia, Dasa and NLR have shown different vortex breakdown characteristics, they predict exactly the same variation of the normal force coefficient. In the pitching moment, the vortex breakdown effects now result in a more complex variation. For the variation of the rolling moment, the agreement of the different solutions is very good, except at the maximum value, where the Dasa solution shows a smaller level. This maximum value is reached during the downstroke motion at about 45°, and the surface pressure contours (Fig. 9) indicate that, at this position, the level of the suction peak on the downward moving part of the wing in the Dasa solution is lower than in the solutions of Alenia and NLR. All solutions show that there is a wide range in which the rolling moment changes sign; it is during the movement from the vertical position to the horizontal position. In this region, there is no longer an aerodynamic damping of the motion.

In the unsteady surface pressure distributions (Fig. 13), the magnitudes now show clearer differences between the upper and lower surfaces. As seen at α=10°, the constant offset and the magnitude of the first and second harmonic show one peak for each half of the wing, at the position of the suction peak of the primary vortex. In the magnitude of the third harmonic, all solutions show a two-peaks shape, where the peaks are now at the pressure gradients inboard and outboard of the suction peak.

The first harmonic is again nearly in phase; there is a phase shift of about 25° only at the mid-section. (There is again the natural phase shift of 180° between upper and lower side.) As the magnitudes of the second and third harmonics in the mid-section region are now larger than in the 10° test case, the phase angles of these harmonics show now a clearer structure. All solutions show a good overall agreement in the prediction of the phase angle of the second harmonic. In the phase angle of the third harmonic, the solutions of DERA and NLR show some common tendencies, whereas the Alenia and the Dasa solutions show some clear deviations from these tendencies.

Most of the differences which are present in the magnitudes and the phase angles in this test case must also be related to the fact that all schemes predict different characteristics of vortex breakdown

Conclusions

The numerical results of CE V show that, taking into account the limitations of the physical model, the flow past the rolling delta wing can be successfully computed by Euler methods. There are some differences between the different methods, but these differences are consistent and depend mainly on the different numerical schemes. At lower angles of incidence, as long as no vortex breakdown is present, the dominating effect is the continuous variation of the local angles of incidence and yaw, overlaid by the antisymmetric flow field of the rolling motion. The differences in the solutions of the different methods are restricted to different levels of the leeward suction peaks; the phase angles are independent of the different schemes.

At higher angles of incidence, in the presence of vortex brake down, there are large time lags in the vortex breakdown relative to the forced motion. The different characteristics of the methods in predicting vortex breakdown result in different instantaneous surface pressure distributions, but again the influence of the different schemes on the phase shift is very small. This independence of the phase shift on the numerical scheme suggests that the phase shift effects are in general predicted correctly by Euler methods.

Acknowledgements

The authors thank the participants in the Technical Co-ordination Group of WEAG TA15 for their co-operation. The computations were carried out by, in addition to the authors, Mr. O. Boelens (NLR)

and Dr. M. Woodgate (University of Glasgow). Special thanks are also due to Prof. D. Hummel (TU Braunschweig), who has contributed very much to CE V by his support in the definition of the model geometry and by numerous technical discussions of the results.

References

[1] Fritz, W.: "WEAG TA 15 Common Exercise V, Numerical and Experimental Investigation of a Delta Wing in Rolling Motion". Final Report, Dasa-Report Dasa/S/STY/1820 (2000).

[2] Arthur, M. T., Kordulla, W., Brandsma, F. J., and Ceresola, N.: "Grid Adaptation in Vortical Flow Simulations", AIAA Paper 97-2308 (1997).

[3] Arthur, M. T., Brandsma, F. J., Ceresola, N. and Kordulla, W.: "Time Accurate Euler Calculations of Vortical Flow on a Delta Wing in Pitching Motion", AIAA Paper 99-3110 (1999).

[4] van der Vegt, J. J. W.: "Time accurate Simulation of Inviscid Compressible Flows with Application to a Pitching Delta Wing", NLR CR 98151 (1998).

[5] Fritz, W.: "Numerical Simulation of Unsteady Vortical Flow about Delta Wings Oscillating at High Incidence", Notes on Numerical Fluid Mechanics, Vol. 72, pp. 162-169, Vieweg Verlag (1999).

[6] Selmin, V.: "The Node-Centred Finite Volume Approach: bridge between Finite Difference and Finite Elements ", Computational Methods Appl. Mech. Engrg., 102, pp 107-138 (1993)

[7] Müller, J. and Hummel, D.: "Time-Accurate CFD Analysis of the Unsteady Flow on a Fixed Delta Wing", AIAA Paper 2000-0138 (2000).

[8] Engler, R., Fonov, S., Klein, C., Bütefisch, K-A., Weiskat, D., Bock, K-W., Fritz, W.: "Study of Unsteady Behaviour of a Rotating 65^{o} Delta Wing at M=0.8 Using Pressure Sensitive Paint (PSP)", Paper A.6 to be presented at RTO/AVT Meeting, Norway, 7th-11th May 2001.

[9] Brandsma F. J., Systma H. A.: "Euler grid to study vortex dynamics on delta wings; grid to be used in WEAG-TA15 Common Exercise V", NLR-CR-99581 (1999).

[10] Hanff, E.S., and Huang, X.Z.: "Roll-Induced Cross-Loads on a Delta Wing at High Incidence", AIAA Paper 91-3223 (1991).

[11] Menzies, M. A. and Kandil, O., A.: "Natural Rolling Responses of a Delta Wing in Transonic and Subsonic Flows", AIAA Paper 96-3391-CP (1993).

[12] Chaderjian, N. M., and Schiff, L. B.: "Numerical Simulation of Forced and Free-to-Roll Delta-Wing Motions", Journal of Aircraft, Vol. 33, No. 1, pp 93-99 (1996)..

[13] Chaderjian, N. M.: "Navier-Stokes Prediction of Large-Amplitude Delta Wing Roll Oscillations", Journal of Aircraft, Vol. 31, No. 6, December 1994 (1994).

[14] Kroll, N., Aumann, P., Bartelheimer, W., Bleecke, H., Eisfeld, B., Lieser, J., Heinrich, R., Kuntz, M., Monsen, E., Raddatz, J., Reisch, U., Roll, B.: "FLOWer Installation and User Handbook", DLR Doc. Nr.: MEGAFLOW-1001 (1998).

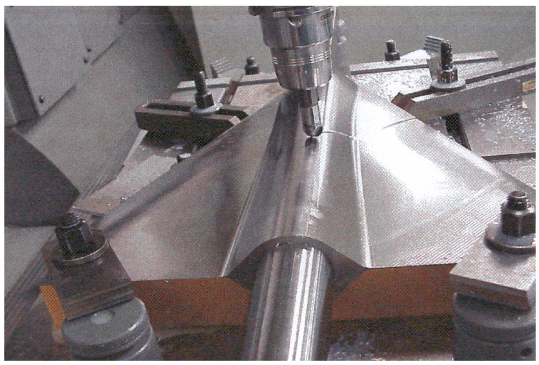

Figure 1: CE V configuration

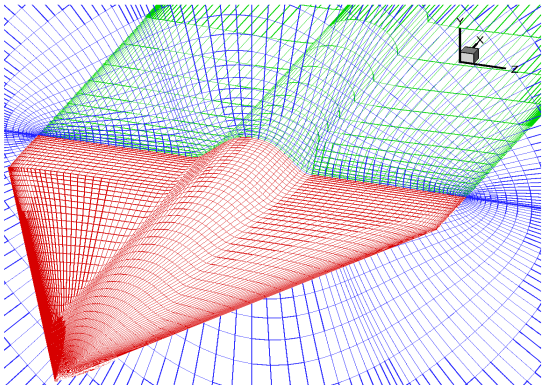

Figure 2: Computational (Euler-) grid

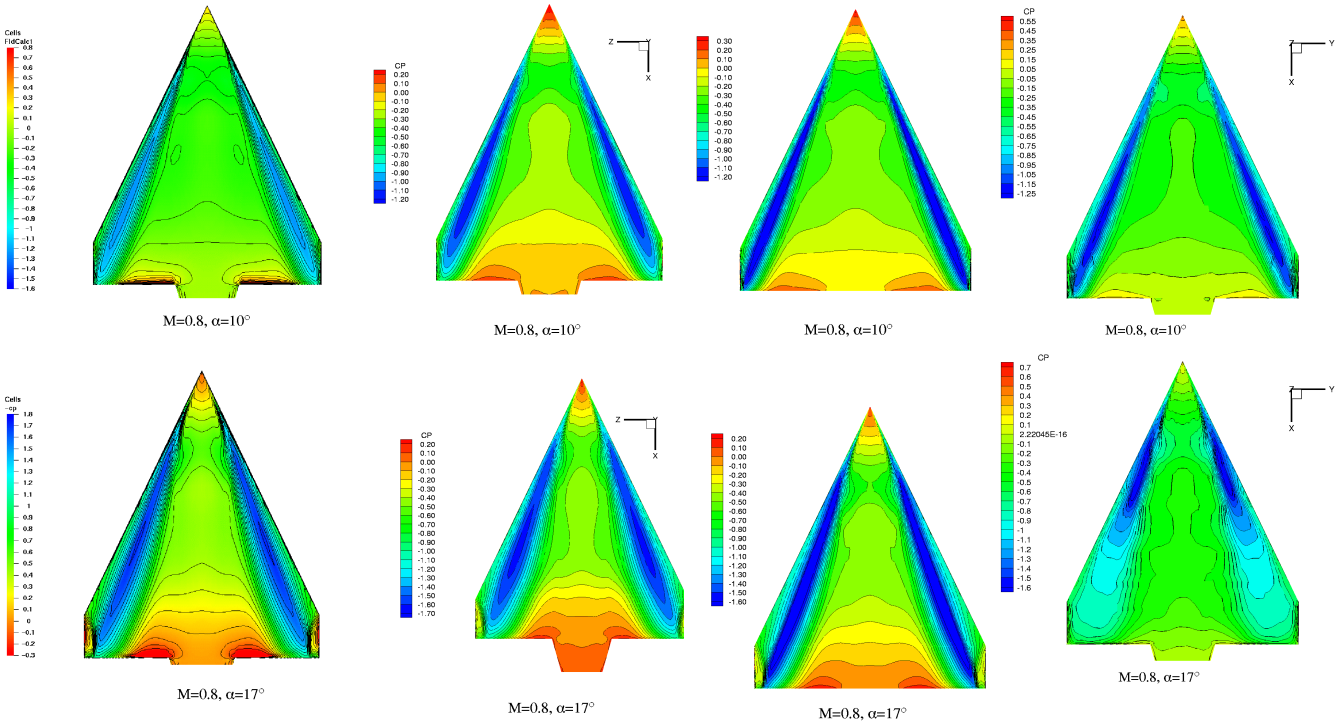

Figure 3: Surface pressure contours of steady solutions for M=0.8, α=10°(upper row) and α=17° (lower row).

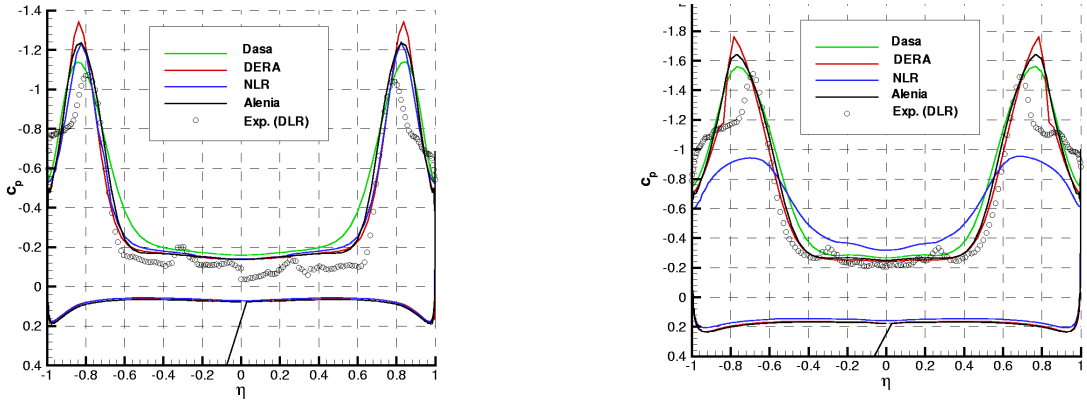

Figure 4: Steady surface pressure distributions at cross section x/c=0.8 for M=0.8, α=10° (left) and α=17° (right).

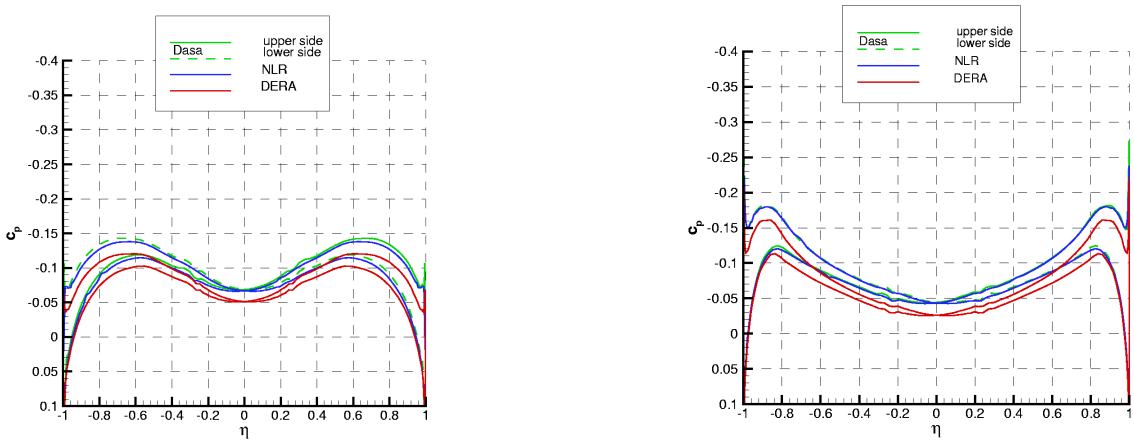

Figure 5: Rolling about body axis at M=0.8, α=0° and ω_r=0.0762. Surface pressure distributions at x/c=0.6 (left) and x/c=0.8 (right).

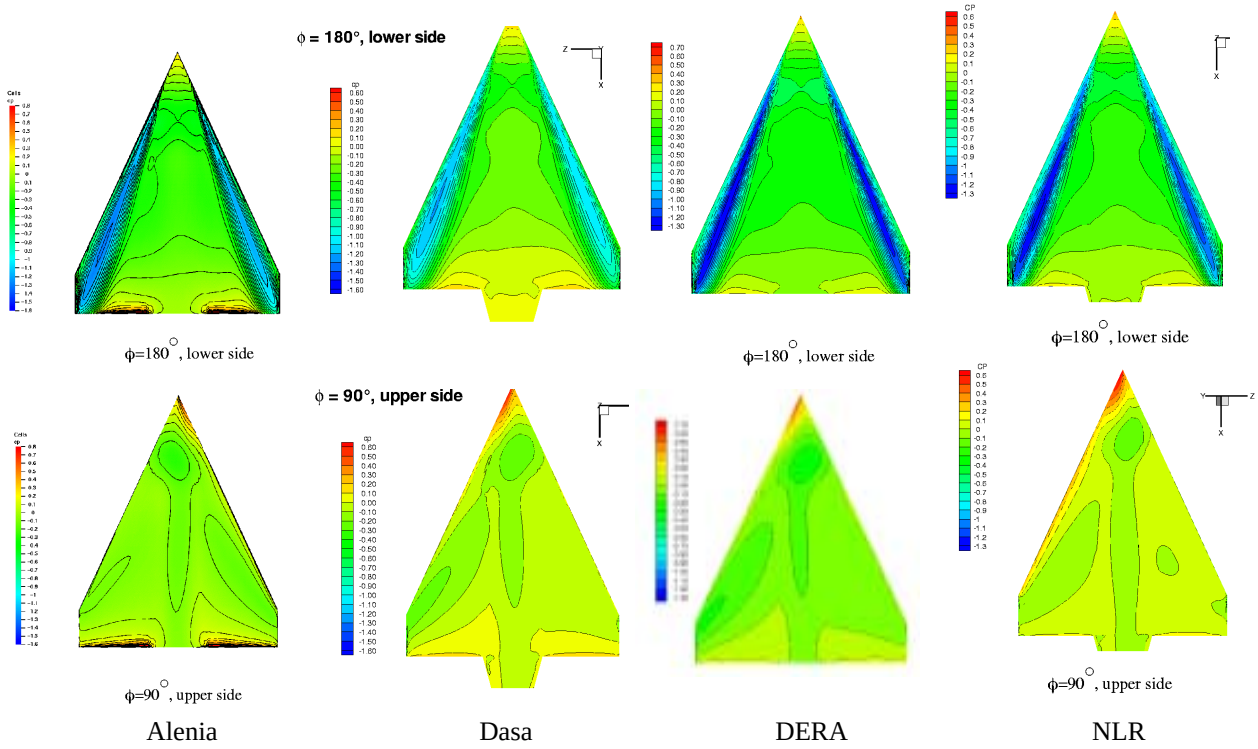

Alenia Dasa DERA NLR

Figure 6: Delta wing rolling about body axis at M=0.8, α=10° and ω_r=0.0762. Instantaneous surface pressure contours at horizontal position (upper row) and vertical position (lower row).

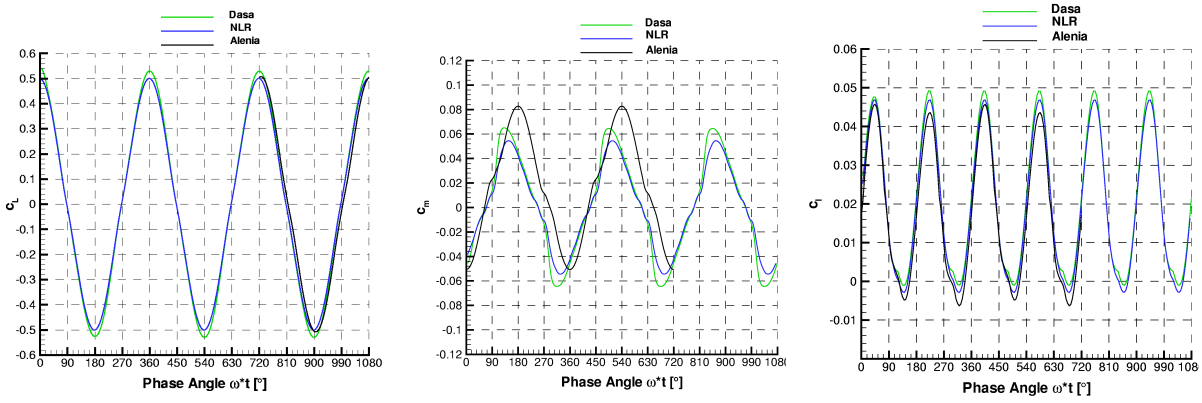

Figure 7: Delta wing rolling about body axis at M=0.8, α=10° and ω_r=0.0762. Variation of lift, pitching- and rolling moment (in body fixed system).

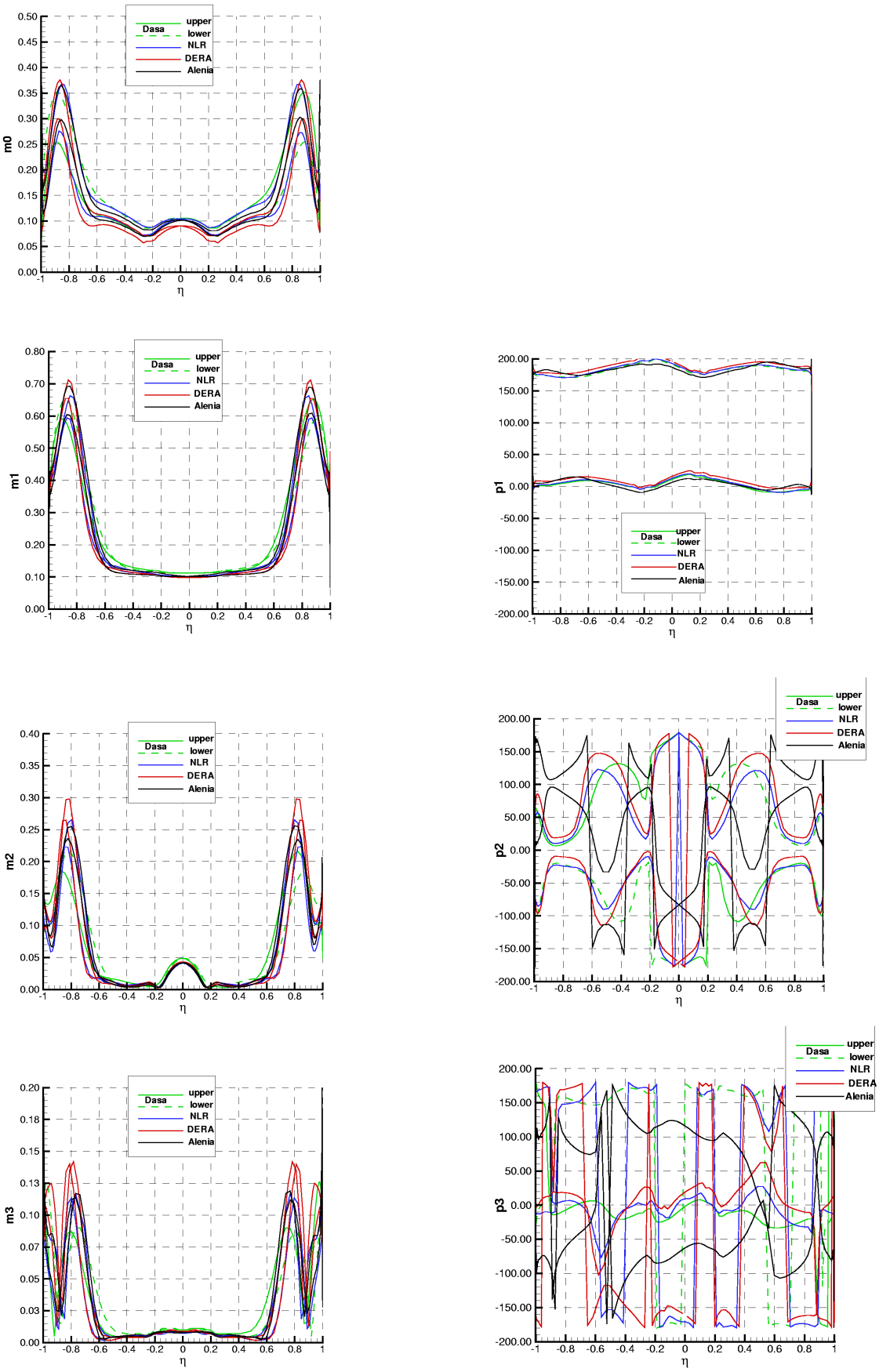

Figure 8: Delta wing rolling about body axis at M=0.8, α=10° and ω_r=0.0762. Unsteady surface pressure distributions as magnitude (m_i) and phase angle (p_i) of the first three harmonics in the cross section x/c=0.8.

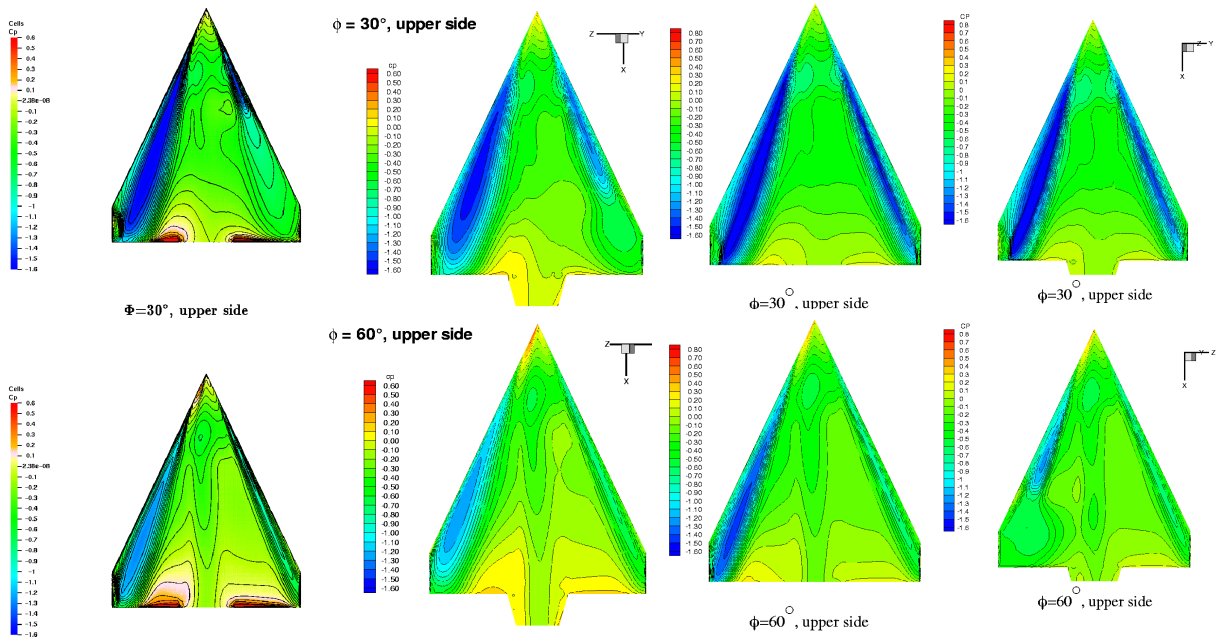

Alenia Dasa DERA NLR

Figure 9: Delta wing rolling about body axis at M=0.8, α=17° and ω_r=0.0762. Instantaneous surface pressure contours during the downstroke motion of the lee side of the wing.

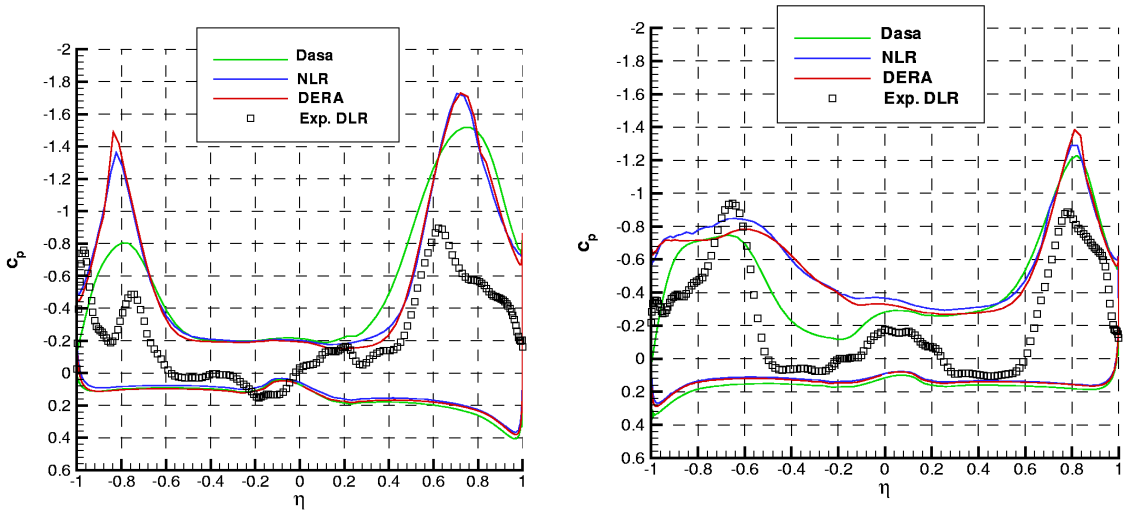

ϕ= 30° **ϕ= 330°**

Figure 10: Delta wing rolling about body axis at M=0.8, α=17° and ω_r=0.0762. Instantaneous surface pressure distributions at different roll angles in the cross section x/c=0.8.

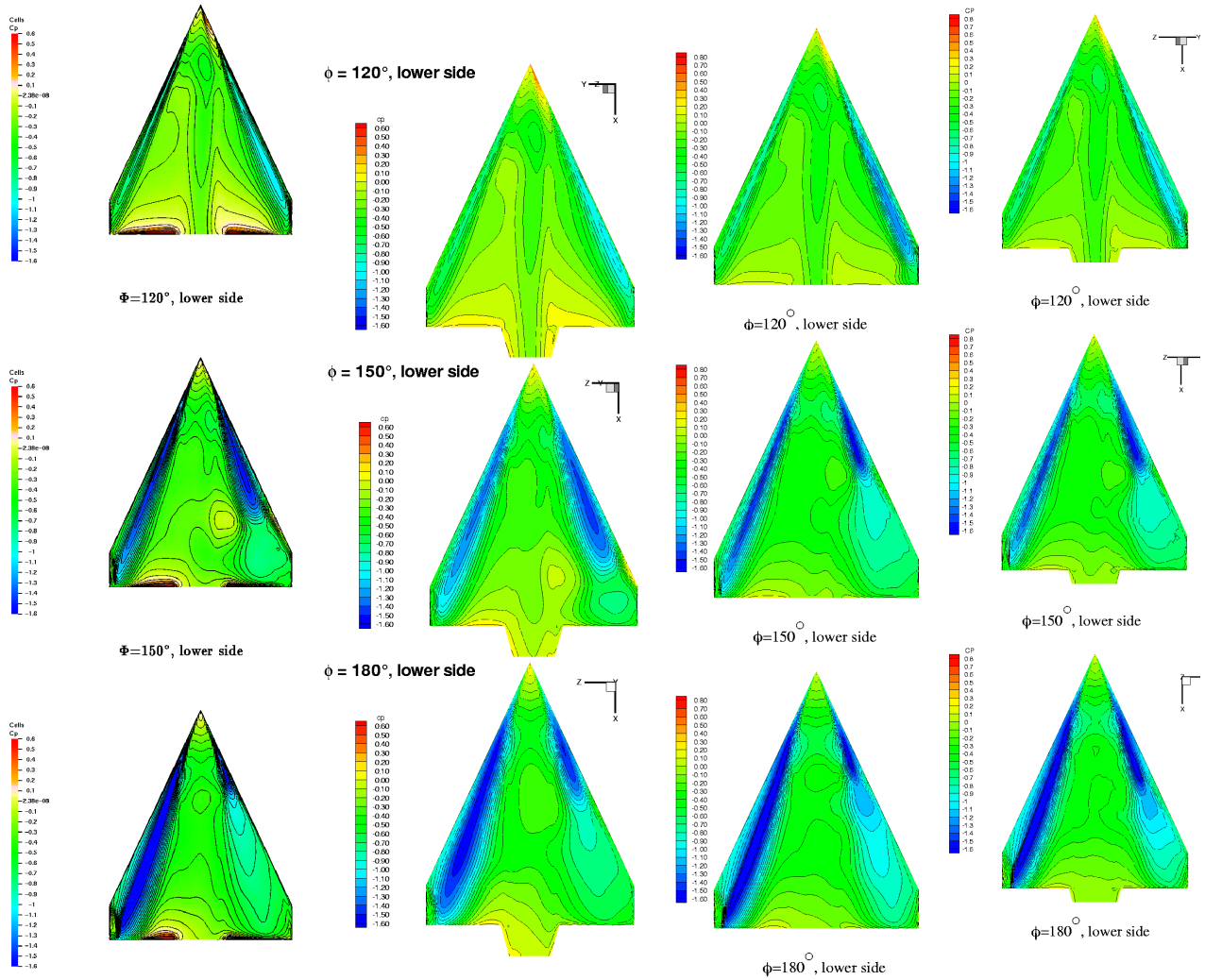

Figure 11: Delta wing rolling about body axis at M=0.8, α=17° and ω_r=0.0762. Instantaneous surface pressure contours during the upstroke motion of the lee side of the wing.

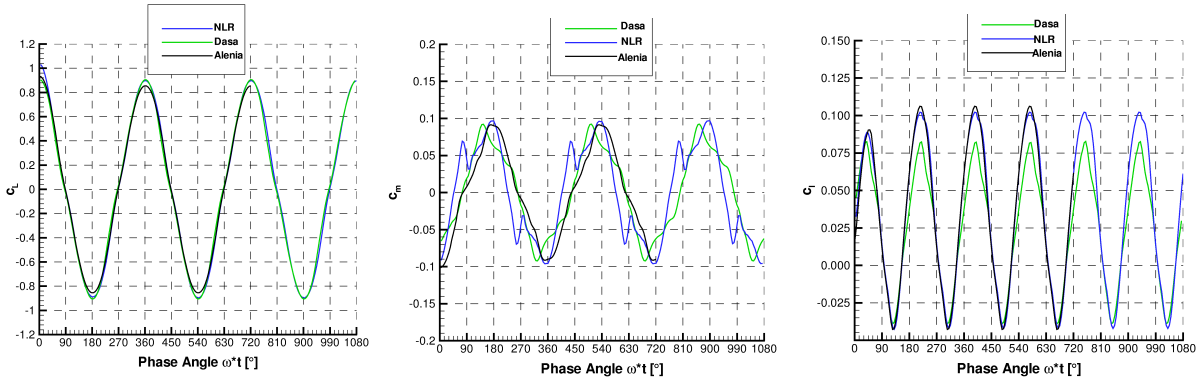

Figure 12: Delta wing rolling about body axis at M=0.8, α=17° and ω_r=0.0762. Variation of lift, pitching- and rolling moment (in body fixed system).

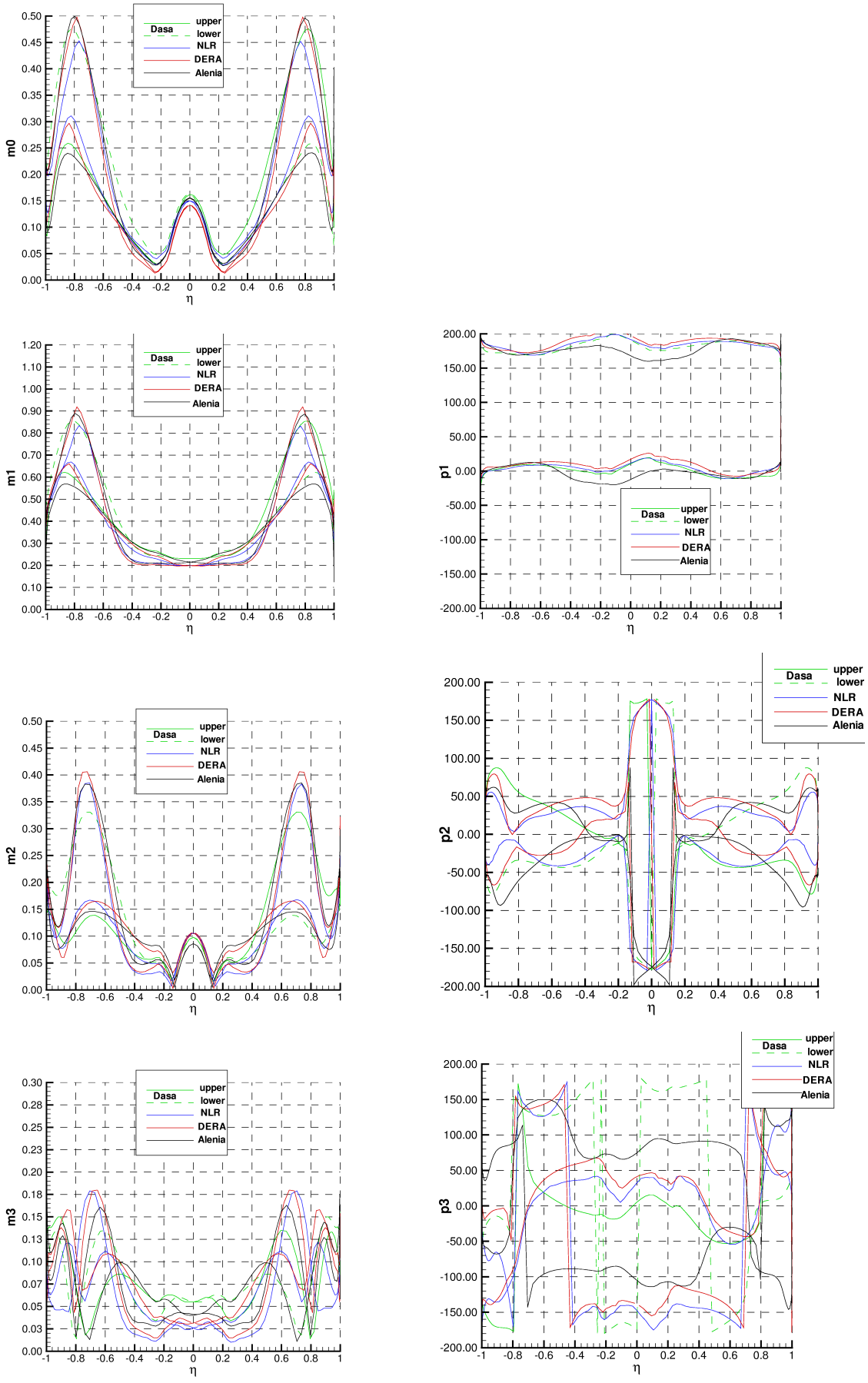

Figure 13: Delta wing rolling about body axis at M=0.8, α=17° and ω_r=0.0762. Unsteady surface pressure distributions as magnitude (m_i) and phase angle (p_i) of the first three harmonics in the cross section x/c=0.8.

Paper: 11
Author: Mr. Fritz

Question by Dr. Hummel: Have the Alenia and Dasa schemes been calibrated with respect to numerical viscosity in order to catch vortex breakdown properly?

Answer: Yes, to some extent.

Question by Dr. Rizzi: Is the good agreement on phase shift among the four results due to the fact that all these methods use the dual-time stepping method?

Answer: It is true that these four methods all use dual-time stepping, but other results (DLR) using a different time integration scheme indicate similar agreement.

This page has been deliberately left blank

Page intentionnellement blanche